https://doi.org/10.31925/farmacia.2023.2.18 **ORIGINAL ARTICLE**

$C_{24}H_{20}N_2O_7$, A NOVEL ISONICOTINAMIDE DERIVATIVE, REGULATES THE PROLIFERATION AND APOPTOSIS OF HepG2 CELLS THROUGH REGULATION OF AUTOPHAGY, ROS PRODUCTION AND THE ER

LING DUAN [1,2], ZHANGPING ZHOU [2], HONGDA LIU [3], ZHUOXUAN LIANG [2], SONG TENG [2], XIAOQIONG HE [2]*, QIAN YAO [4]

[1]*Department of clinical Nutrition, The First People's Hospital of Yunnan Province, the Affiliated Hospital of Kunming University of Science and Technology, Kunming, 650032, China*
[2]*School of Public Health, Kunming Medical University, Kunming, 650500, China*
[3]*School of Nursing, Kunming Medical University, Kunming, 650500, China*
[4]*Department of Yunnan Cancer Center, The Third Affiliated Hospital to Kunming Medical University, Kunming, 650100, China*

**corresponding author: hexqcn@aliyun.com*

Manuscript received: November 2022

Abstract

This study explored the anticancer activity of $C_{24}H_{20}N_2O_7$ [(E)-N-(1-(6-acetyl-7,9-dihydroxy-8,9b-dimethyl-1,3-dioxo-3,9b-dihydrodibenzo [b,D]furan-2(1-h)-alkylene)ethyl)isonicotinamide], a novel chemical compound modified by esterification of $C_{18}H_{17}NO_6$. MTT assays, colony formation assays, and flow cytometry analyses were performed to investigate the effect of $C_{24}H_{20}N_2O_7$ on the proliferation and apoptosis of HepG2 cells *in vitro*. A xenograft model in nude mice using HepG2 cells was established to validate the effects of $C_{24}H_{20}N_2O_7$ *in vitro*. The results revealed that the proliferation inhibition rate and the apoptosis rate of HepG2 cells were significantly increased *in vitro* compared with the control group. $C_{24}H_{20}N_2O_7$ treatment also inhibited the volume and mass of HepG2 cell mouse xenografts *in vivo*, and the body weight and the primary organ coefficient did not differ significantly from the control group. $C_{24}H_{20}N_2O_7$ may exert its effects through regulation of autophagy, reactive oxygen species, and endoplasmic reticulum regulated apoptosis. These results indicated that $C_{24}H_{20}N_2O_7$ inhibited the proliferation of HepG2 cells and promoted their apoptosis, whilst exhibiting low toxicity *in vitro* and *in vivo*.

Rezumat

În cadrul acestui studiu am evaluat activitatea anticancerigenă a $C_{24}H_{20}N_2O_7$ [(E)-N-(1-(6-(6-acetil-7,9-dihidroxi-8,9b-dimetil-1,3-dioxo-3,9b-dihidrodibenzo [b,D]furan-2(1-h)-alchilen)etil)izonicotinamidă], un compus chimic nou obținut prin esterificarea $C_{18}H_{17}NO_6$. S-au efectuat teste MTT, teste de formare de colonii și analize prin citometrie în flux pentru a investiga efectul $C_{24}H_{20}N_2O_7$ asupra proliferării și apoptozei celulelor HepG2 *in vitro*. Pentru a valida efectele $C_{24}H_{20}N_2O_7$ *in vitro*, a fost stabilit un model de xenografă la șoareci folosind celule HepG2. Rezultatele au arătat că rata de inhibare a proliferării și rata de apoptoză a celulelor HepG2 au crescut semnificativ *in vitro* în comparație cu grupul de control. Tratamentul cu $C_{24}H_{20}N_2O_7$ a inhibat, de asemenea, volumul și masa xenografelor la șoareci, iar greutatea corporală nu a fost semnificativ diferită față de grupul de control. $C_{24}H_{20}N_2O_7$ își poate exercita efectele prin reglarea autofagiei, a speciilor reactive de oxigen și a apoptozei. Aceste rezultate au indicat că $C_{24}H_{20}N_2O_7$ a inhibat proliferarea celulelor HepG2 și a indus apoptoza acestora, prezentând în același timp o toxicitate scăzută *in vitro* și *in vivo*.

Keywords: $C_{24}H_{20}N_2O_7$, liver cancer, HepG2, anticancer, autophagy, reactive oxygen species, endoplasmic reticulum

Introduction

Primary liver cancer (PLC) is a common malignant tumour of the digestive system, the incidence of which is increasing [1]. Hepatocellular carcinoma (HCC) plays an important role in PLC. According to the 2019 national cancer report [2], liver cancer remains the most common malignant tumour in China. Approximately 80% of HCC patients have no surgical indications as they are diagnosed with advanced-stage HCC. Chemotherapy has become an important approach for such patients. Traditional Chinese Medicines are used to treat several different types of cancers with good therapeutic effects and low toxicity [3, 4]. However, several Traditional Chinese Medicines are underutilized due to their poor solubility and low bioavailability [5, 6].

Our previous research found a novel, natural anticancer drug $C_{18}H_{17}NO_6$ [6-acety1-2-(1-amino-ethylidene)-7, 9-dihydroxy-8, 9b-dimethy1-9bH-dibenzofuran-1, 3-dione] with low toxicity, which had been extracted from a Traditional Chinese Medicine [7, 8]. The drug significantly inhibited the proliferation of several different cancer cells, including liver cancer cell lines,

lung cancer cell lines, and nasopharyngeal carcinoma cells (patent ID: 201710388136.8). However, it suffers from poor solubility. Based on the fact that curcumin succinate and milk proteins became soluble after esterification [9], $C_{24}H_{20}N_2O_7$ [(E)-N-(1-(6-acetyl-7,9-dihydroxy-8,9b-dimethyl-1,3-dioxo-3,9b-dihydrodi-benzo [b,D]furan-2(1-h)-alkylene)ethyl)isonicotin-amide] was developed by esterification of $C_{18}H_{17}NO_6$. Acute toxicity experiment, 30-day feeding experiments, sperm deformity experiments and micronuclei experiments were performed using mice, and the results showed that mice only developed nephrotoxicity at high doses (2.6 g/kg), and otherwise the esterified compound was safe [10]. The present study used human HepG2 cells and BALB/c nude mice to investigate the anti-cancer effects of $C_{24}H_{20}N_2O_7$. The aim of the present study was to provide a reference for the further study of Traditional Chinese Medicines with regard to their chemotherapeutic efficacy.

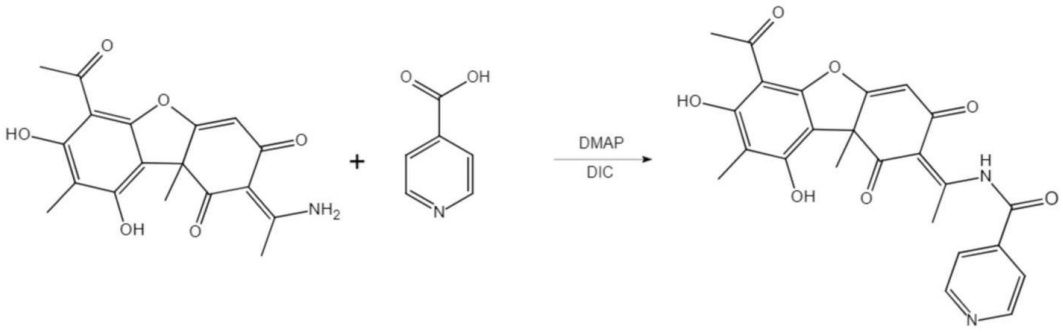

Figure 1.
Formation of $C_{24}H_{20}N_2O_7$. $C_{18}H_{17}NO_6$ and 4-picolinic acid were used as reactants, 4-dimethylaminopyridine (DMAP) and N'-diisopropylcarbodiimide (DIC) were used as catalysers. An isonicotinic acid group was added to the structure of $C_{18}H_{17}NO_6$ after esterification.

Materials and Methods

Preparation of $C_{24}H_{20}N_2O_7$

The chemical reaction which underlies the formation of $C_{24}H_{20}N_2O_7$ is shown in Figure 1. $C_{18}H_{17}NO_6$ and 4-picolinic acid were used as reactants, DMAP and DIC were used as catalysts. In addition, the products were purified by column chromatography until the purity of $C_{24}H_{20}N_2O_7$ was found to be > 95%. The concentration of $C_{24}H_{20}N_2O_7$ solution was 10 mM and was dissolved in dimethyl sulfoxide (DMSO). Culture medium was used to dilute the compound for the subsequent experiments.

Cell culture and cell treatment

HepG2 liver cancer cells were kindly provided by the Yunnan Cancer Center and were originally purchased from the Cell Bank of Kunming Animal Institute, Chinese Academy of Science. All cells were maintained in complete medium; DMEM/F-12 (1:1) (Basalmedia) supplemented with 10% foetal bovine serum (FBS) (Biological Industries), 1% streptomycin (100 µg/mL) and penicillin (100 U/ mL). Cells were cultured in a humidified incubator at 37°C supplied with 5% CO_2. The cells were passaged when 80 - 90% confluence was achieved.

MTT assay

Each well of the 96-well plates were seeded with 3 x 10^3 cells, then cultured overnight. 0.625, 1.25, 2.5, 5, 10 µM $C_{24}H_{20}N_2O_7$ were used to treat the cells for 24, 48, or 72 h. The monolayers were incubated in standard conditions of culture with 5 mg/mL 3-(4,5-di-methylthiazol-2-yl)-2,5-diphenyltetrazolium bromide (MTT) (BioFroxx) solution prepared in complete medium. After 4 h the formazan crystals were solubilized with 0.1% DMSO for 5 - 10 minutes. Then measured the optical density of the different groups of cells was at 490 nm by Multiskan Spectrum (Thermo Fisher Scientific, Inc.). The formula for calculation of cell viability was:

$$\text{Cell viability (\%)} = [(ODe - ODb)/(ODc - ODb)] \times 100,$$

where, Ode is the experimental group absorbance value, ODb is the blank group absorbance value, and ODc is the control group absorbance value.

Colony formation assays

A total of 200 cells were seeded into each well of a 6 well culture plate and allowed to adhere overnight (37°C, 5% CO_2). The following day, the media was replaced with 2 mL fresh medium containing different concentrations of the drugs (0.625, 1.25, 2.5 µM). Plates were incubated for a further 9 days, with medium replace on days 3 and 6, whilst colony formation was monitored by inverted optical microscope (OLYMPUS). Media was removed on the 9th day, and each well was washed once with 2 mL phosphate buffered saline (PBS) (Biological Industries) and fixed with 5% paraformaldehyde (Fengchuang) for 15 min at room temperature (RT). Wells were then washed with 2 mL PBS, stained with 0.5 mL 0.5% crystal violet for 10 min, and washed again with 2 mL PBS before acquiring pictures with a camera

(Huawei P30) and counting the number of colonies. The inhibition rate was calculated as follows:

$$\text{Inhibition rate} = [(Nc - Nd)/Nc] \times 100,$$

where, Nc is the number of colonies in the vehicle control group, and Nd is the colony number in the drug group.

Apoptosis assay

A total of 4 x 10^5 cells were seeded in a 25 cm^2 culture flask and cultured overnight. 1.5, 3 and 6 μM $C_{24}H_{20}N_2O_7$ were added to treat cells for 48 h. Next, added 1 mL Trypsin (Biological Industries) in each culture flask for 2 minutes to detached cells from the culture surface, the cells and supernatant were centrifuged (500x g, 5 min, RT) after harvesting, and the cells were resuspended in 1 x binding buffer. Next, 400 μL of the cell suspension was incubated with 5 μL Annexin-FITC in the dark for 15 min at RT, then 10 μL PI was added and the cells were further incubated in the dark on ice for 5 min. All reagents used were part of the Annexin V-FITC/PI apoptosis kit (7 sea Biotech). Cell apoptosis was measured using a Dx-Flex flow cytometry (Beckman Coulter, Inc.).

Transcriptome sequencing

Seeded 1 × 10^6 HepG2 cells in each 75 cm^2 culture flask for 24 h. then cells were treated with 1.5, 3, 6 μM $C_{24}H_{20}N_2O_7$ for 48 h. After washing twice with cold PBS, total RNA was rapidly extracted from the cells using TRIzol®, and samples were stored at -80˚C. Samples were shipped to Shanghai Qi Ming Biological Information Ltd. for RNA quality and gene expression profiling analysis. HISAT2 [11, 12] was used to align the reference genes, and analysis of gene expression levels and their differences were determined using STRINGTIE and DESeq2 [13]. Gene expression enrichment analyses were performed using GO (Gene Ontology) [14, 15] and KEGG (Kyoto Encyclopedia of Genes and Genomes) [16] using the Gene Cloud Biotechnology Information (GCBI) software. Genes were filtered by fold change (FC) value of $0.67 < \log_2(FC) < 1.5$ and $p < 0.05$ based on a Student's t-test.

Tumour growth model in nude mouse

The animal experiments performed in the present study were approved by the Ethical Committee of Kunming Medical University (No. KMMU2020393, Kunming, China). Animal care was performed in accordance with guidelines for laboratory animal ethical (GB/T 35892-2018), all animals were kept in Specific Pathogen Free (SPF) level laboratory animal room, and all animal experiment operators have obtained animal experimental qualification certificates. Two indicators were combined to determine humane end-points in this study: (1) tumour volume grows up to 2000 mm^3; (2) the loss of body weight up to 20%. A total of 2 x 10^6 HepG2 cells cultured in medium were implanted into 32 BALB/c nude mice (6 - 8 weeks, male, Beijing Vital River Laboratory Animal Technology Co., Ltd.) by subcutaneous injection. After 14 days, the mice were randomly divided into different groups; physiological saline control group, 10, 20, 40 mg/kg $C_{24}H_{20}N_2O_7$ groups, and a 2 mg/kg cisplatin (DDP) group when tumours grew to 200 mm^3. There were 6 mice in each group. Mice were treated by intraperitoneal injection once a day, and subsequently the body weight and tumour volume were measured. After 23 days of treatment, the tumours and major organs were obtained by dissection following cervical dislocation, while verifying the animal's death by the loss of breathing, heartbeat and nerve reflexes. The formulas for calculation of relative tumour volume (RTV), the relative proliferation ratio (RPR), and the organ coefficient were:

$$\text{Tumour volume} = (a \times b^2)/2,$$

where, a is the longer diameter and b is the shorter diameter; RTV = volume at measuring/volume at grouping; RPR = TRTV/CRTV, where TRTV is the RTV of the drug group and CRTV is the RTV of the vehicle control group.

$$\text{Tumour inhibition rate (\%)} = (Mc - Md)/Mc \times 100,$$

where, Mc is the tumour weight of the vehicle control group and Md is the tumour weight of the drug group; and organ coefficient = organ weight/body weight.

Statistical analysis

Each cell experiment was repeated 3 times. All experimental data were analysed using SPSS version 21.0 (IBM Corp) and GraphPad Prism version 7.0 (GraphPad Software, Inc.). Data are presented as the mean ± standard deviation. A one-way ANOVA followed by a post-hoc Dunnett's t-test were used to compare differences. $p < 0.05$ was considered to indicate a statistically significant difference.

Results and Discussion

Effects of $C_{24}H_{20}N_2O_7$ on the viability of HepG2 cells in vitro

MTT and colony formation assays were used to investigate the effect of $C_{24}H_{20}N_2O_7$ on the proliferation of HepG2 cells *in vitro*. The results indicated that $C_{24}H_{20}N_2O_7$ had an inhibitory effect on HepG2 cell proliferation, and its effect was dose and time-dependent (Figure 2A). The IC_{50} at 24, 48 and 72 h were 8.40 ± 0.87, 4.30 ± 0.57 and 3.09 ± 0.86 μM respectively. The inhibition rates of colony formation were 25.48 ± 1.91%, 64.01 ± 1.46%, and 100% when treated with 0.625, 1.25 and 2.5 μM of the compound. Similarly, the inhibitory effects of $C_{24}H_{20}N_2O_7$ were dose and time-dependent (Figure 2B).

An inverted microscope was used to observe HepG2 cells treated with $C_{24}H_{20}N_2O_7$, the cells exhibited a crumpled and deformed morphology, and some cells became smaller, more rounded, and a large number of fragments floated in the culture medium (Figure 3).

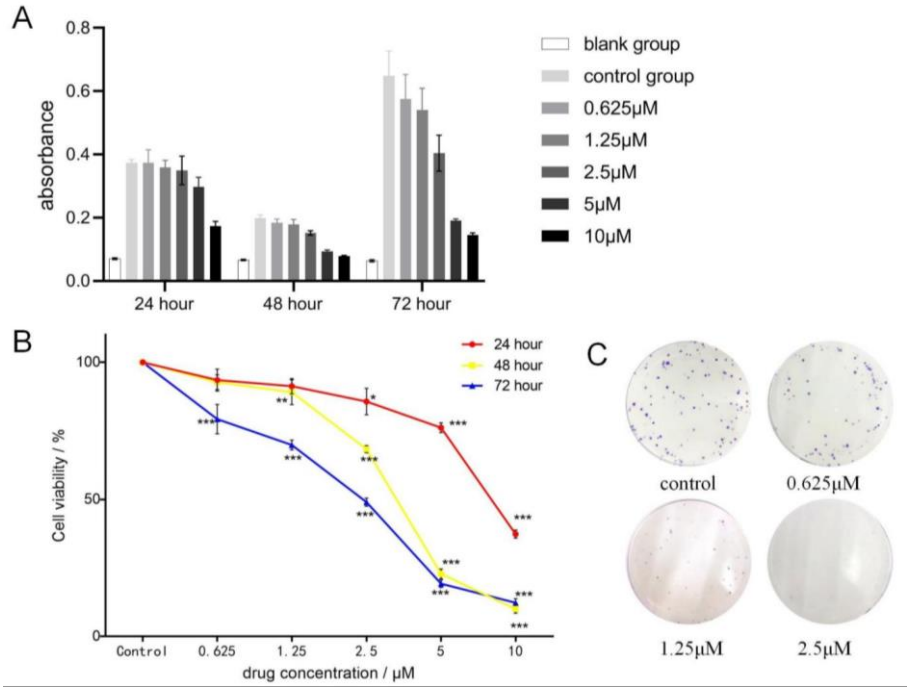

Figure 2.

Inhibitory effect of $C_{24}H_{20}N_2O_7$ on HepG2 cell viability. (A) The absorbance of the treated samples for MTT assay. (B) Viability of HepG2 cells after $C_{24}H_{20}N_2O_7$ treatment for different lengths of time and with different concentrations. (C) Representative examples of colony growth of HepG2 cells treated with different concentrations of $C_{24}H_{20}N_2O_7$ for 9 days, cells were stained with crystal violet, the numbers of visible colonies with more than 50 cells per colony (phone camera)

Data are presented as the mean ± SD, *p < 0.05, **p < 0.01, ***p < 0.001 *vs*. control

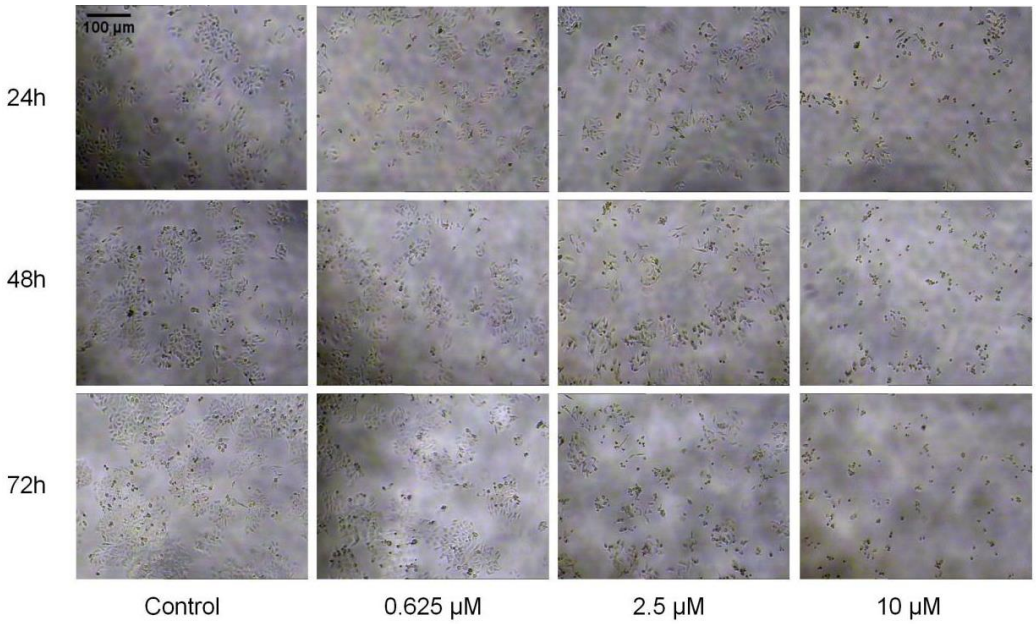

Figure 3.

Morphological changes of the HepG2 cells after treatment with $C_{24}H_{20}N_2O_7$ for different lengths of time and with different concentrations (magnification, x100).

Effects of $C_{24}H_{20}N_2O_7$ on apoptosis of HepG2 cells in vitro

HepG2 cell apoptosis was detected using flow cytometry. As shown in Figure 4, compared with the control group, the apoptotic ratio of HepG2 cells based on flow cytometry analysis was notably increased in cells treated with $C_{24}H_{20}N_2O_7$. The apoptotic ratios in the control group, 1.5 μM group, 3 μM group and

6 μM group were 6.44 ± 0.33%, 7.87 ± 0.48%, 10.28 ± 0.32% and 18.50 ± 0.84%, respectively.

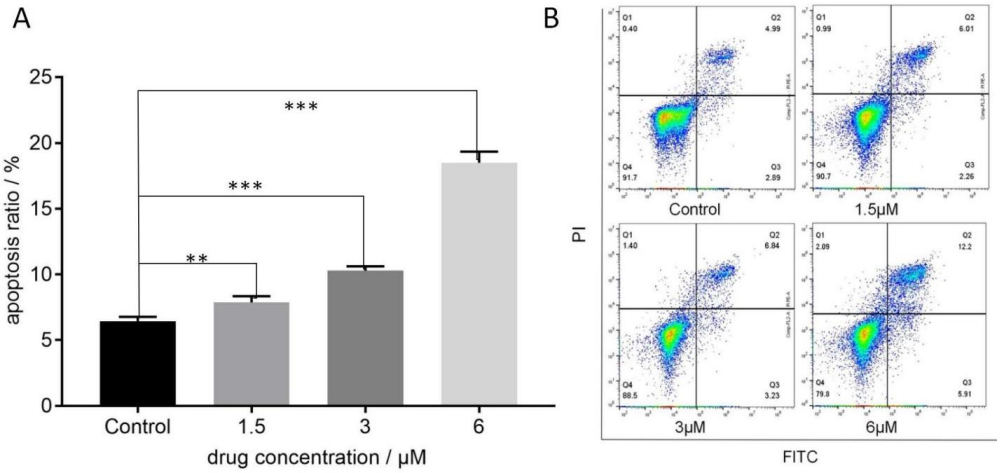

Figure 4.

The effects of $C_{24}H_{20}N_2O_7$ on apoptosis of HepG2 cells were assessed using flow cytometry. (A) Quantification of the total apoptotic rates in HepG2 cells treated with different concentrations of $C_{24}H_{20}N_2O_7$. (B) Representative FACS analysis of apoptosis of HepG2 treated with $C_{24}H_{20}N_2O_7$

** $p < 0.01$, *** $p < 0.001$ *vs*. control

Transcriptome sequencing

Gene expression profiling revealed that $C_{24}H_{20}N_2O_7$ significantly modulated several canonical signalling pathways associated with autophagy, as well as with reactive oxygen species (ROS) and the endoplasmic reticulum (ER), amongst others. ATG13 was the unique representative enriched in autophagy pathways. SOD2 upregulation resulted in increased ROS production and this ultimately led to apoptosis. GO analysis showed the biological processes, cell components and molecular functions associated with the endoplasmic reticulum that were significantly modulated by 6 μM $C_{24}H_{20}N_2O_7$. The effect of $C_{24}H_{20}N_2O_7$ on gene expression showed a dose-response relationship (Figure 5A and 5B). A total of 6 differentially downregulated genes (shown in Figure 5C) ACER3, GPR78, IDH3A, RAB43, RPS6KA1 and TICRR were found to be associated with $C_{24}H_{20}N_2O_7$ treatment. A schematic diagram of the proposed mechanism by which $C_{24}H_{20}N_2O_7$ exerts its anticancer activity in HepG2 cells is shown in Figure 6.

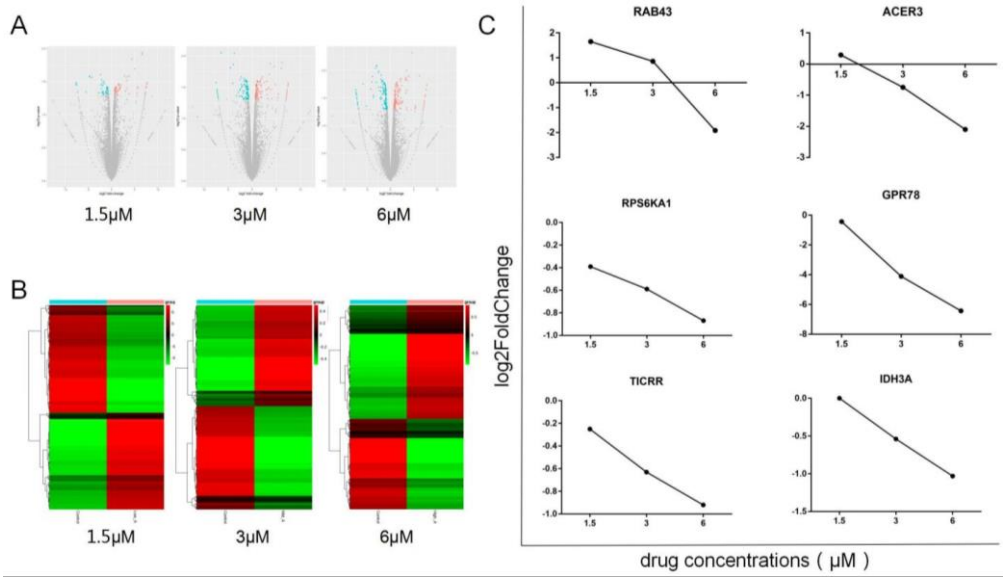

Figure 5.

$C_{24}H_{20}N_2O_7$ regulates the expression of genes in HepG2. (A) Volcano plot of gene expression. (B) Heatmap of gene expression. (C) Changes in the expression of 6 differentially downregulated genes that favour anticancer activity following treatment with $C_{24}H_{20}N_2O_7$.

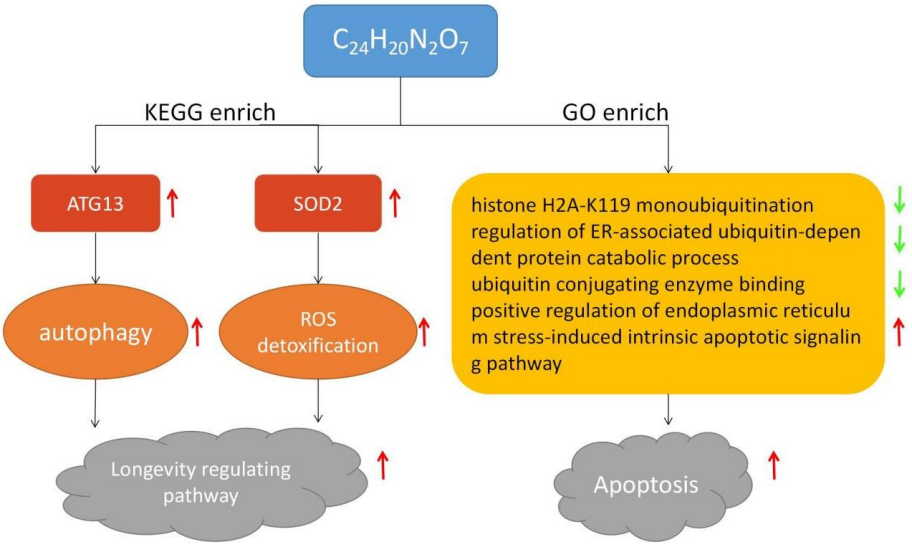

Figure 6.

Schematic diagram of the proposed mechanism of action of $C_{24}H_{20}N_2O_7$. $C_{24}H_{20}N_2O_7$ regulates the expression of genes favouring anticancer activity, in which ATG13 mediated autophagy pathways; SOD2 activity, ROS activity and endoplasmic reticulum are upregulated. ROS, reactive oxygen species.

Effects of $C_{24}H_{20}N_2O_7$ on tumour growth in vivo

To further investigate the effects of $C_{24}H_{20}N_2O_7$ on inhibiting the proliferation of HepG2 cells *in vivo*, an HepG2 cell xenograft model was established using nude mice to validate the *in vitro* findings. Compared with the control group, the RTV, RPR, and the weight of the tumour were significantly reduced *in vivo*. The RTV of the 40 mg/kg group and DDP (2 mg/kg) group differed significantly from the control group after 11 days, and the 20 mg/kg group had a similar difference after 17 days (Figure 7A). The RPR of the 10, 20, and 40 mg/kg groups were 68.72%, 49.29%, and 39.16%, respectively after 23 days (Figure 7B). $C_{24}H_{20}N_2O_7$ also inhibited the growth of the tumour based on the weights; the tumour inhibition rates of the 10, 20, and 40 mg/kg groups were 15.56 ± 2.55%, 32.69 ± 2.91%, and 48.39 ± 1.40%, respectively (Figure 7C).

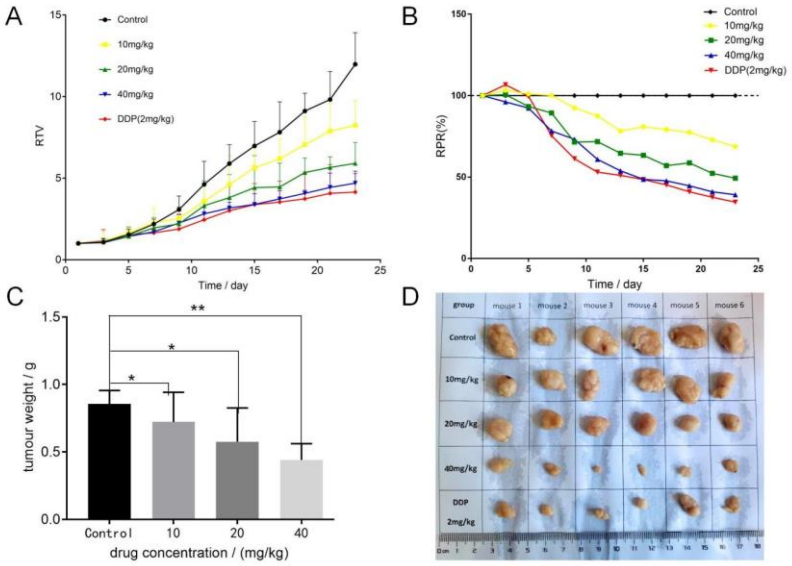

Figure 7.

Effects of $C_{24}H_{20}N_2O_7$ on HepG2 xenograft growth in nude mice. (A) RTV in the different groups throughout the study. Data were compared using a one-way ANOVA. n = 6. (B) RPR of the tumour in different groups throughout the study. (C) Tumour weight at the end of the study. (D) Representative pictures of tumour after different treatments. Data are presented as the mean ± SD

*p < 0.05, **p < 0.01 *vs.* control. RTV, relative tumour volume; RPR, relative proliferative rate

Effects of $C_{24}H_{20}N_2O_7$ on the body weight and major organ coefficient of the mice

The body weights of mice were recorded, and the weights of the liver, spleen, kidney, and testis were measured following dissection after cervical dislocation. As shown in Figure 8, the body weights of the mice were not impacted by $C_{24}H_{20}N_2O_7$ treatment. However, the body weights in the DDP group did decrease compared with the control group after 9 days (Figure 8A). There was no difference in the organ coefficients between the $C_{24}H_{20}N_2O_7$ groups and the control group; only the DDP group had a significant difference in the coefficient for the kidneys and testes (Figure 8B).

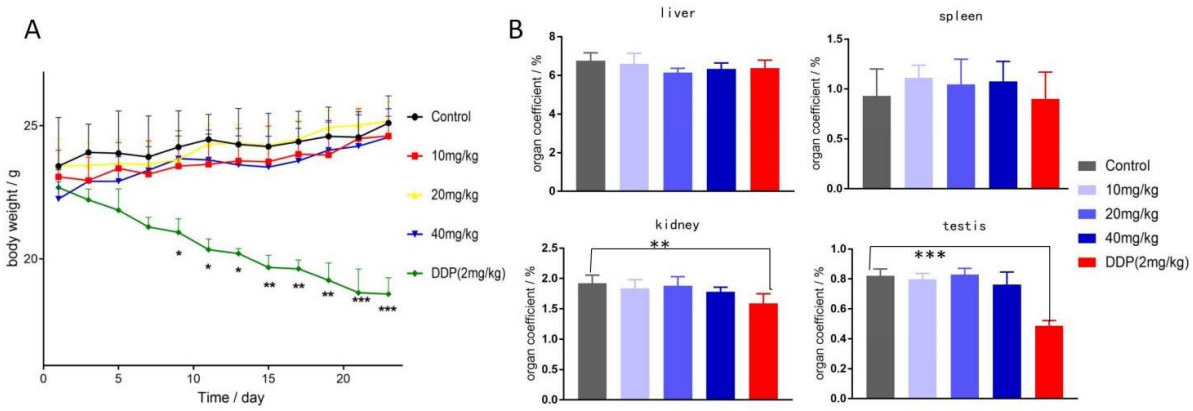

Figure 8.

Effects of $C_{24}H_{20}N_2O_7$ on the body weights and organ coefficients in nude mice (A) Changes in the weight of mice throughout the study. (B) Organ coefficients of the liver, spleen, kidney, and testis at the end of the study. Data are presented as the mean ± SD

*p < 0.05, **p < 0.01, ***p < 0.001 *vs.* control

The isonicotinic acid group was added to the structure of $C_{18}H_{17}NO_6$ after esterification, and our previous experiments confirmed the solubility of $C_{24}H_{20}N_2O_7$ in 75% ethanol and n-octanol was higher than that of $C_{18}H_{17}NO_6$. Which is in agreement with other authors, who demonstrated that naringin was esterified by oleic acid to improve its solubility [17]. In our study, we improved the solubility of $C_{18}H_{17}NO_6$ in ethanol and n-octanol, but it's still not ideal in water. Next, we can refer to other researches to solve the problem of poor solubility by developing nanosized drug delivery system or nano-liposomes [18-20].

The present study indicated that $C_{24}H_{20}N_2O_7$ reduced the proliferation of HepG2 cells and induced their apoptosis *in vitro* and *in vivo*. The compound exerted its effects through the regulation of autophagy, ROS levels and ER-related mechanisms. The stabilization of ATG13 is closely associated with autophagy [17], excessively ubiquitinated ATG13 protein was recruited to the phagosome for prolonged expansion, and therefore inhibits autophagosome maturation. In the present study, ATG13 expression was significantly upregulated when treated with $C_{24}H_{20}N_2O_7$, thus promoting the anticancer activity of the compound in HepG2 cells. ATG13 expression levels were altered following $C_{24}H_{20}N_2O_7$ treatment in a concentration-dependent manner. ROS are chemically reactive chemical species containing oxygen, which have a synergistic effect following chemotherapy to kill cancer cells whilst preserving normal cells to avoid/reduce the side effects of anticancer drugs [21]. SOD2 promotes the effects of ROS, which in turn affects a cell's lifespan. Other study have shown that a Pyrazolate Osmium(VI) Nitride induces apoptosis through promoting HepG2 cells to release ROS [22]. These proteins are also the chemotherapeutic targets of cephalosporin antibiotics against cancers [23]. Protein handling, modification, and folding in the ER are tightly regulated processes that determine cell function, fate, and survival [24]. $C_{24}H_{20}N_2O_7$ induced ER-stress in HepG2 cells and thus promoted apoptosis.

Cancer is recognized by distinct abnormalities and/or dysregulation of various genes, which results in sustained proliferative signalling, evasion of growth suppression, activation of invasion and metastasis, replication immortality, induction of angiogenesis, and resistance to cell death [25-30]. In the present study, ACER3, GPR78, IDH3A, RAB43, RPS6KA1 and TICRR were reported to be closely associated with the anticancer effects of, and were significantly regulated by $C_{24}H_{20}N_2O_7$ in HepG2 cells. Their expression levels were downregulated as the concentration of $C_{24}H_{20}N_2O_7$ increased, consistent with the anticancer efficacy of $C_{24}H_{20}N_2O_7$ both *in vitro* and *in vivo*. Regulation of these genes may contribute to the anticancer activity on HepG2.

Comparing the inhibitory effects of $C_{24}H_{20}N_2O_7$ and $C_{18}H_{17}NO_6$ on HepG2 cells *in vitro*, the IC_{50} of

$C_{24}H_{20}N_2O_7$ was higher than that of $C_{18}H_{17}NO_6$, indicating $C_{24}H_{20}N_2O_7$ still has a strong anti-cancer effect after esterification *in vitro*. Moreover, the inhibition rates on HepG2 tumours *in vivo* showed that the effects of $C_{18}H_{17}NO_6$ was Stronger inhibited than $C_{24}H_{20}N_2O_7$ [7, 8]. The differences in the anti-tumour effects between $C_{24}H_{20}N_2O_7$ and $C_{18}H_{17}NO_6$ may thus be related to the underlying mechanisms regulated by each compound.

Conclusions

In conclusion, esterification increased the solubility of the drug and improved its bioavailability, and this may serve as a reference for other related studies/ compounds. Comparing the antitumor effects of $C_{24}H_{20}N_2O_7$ and DDP *in vivo*, $C_{24}H_{20}N_2O_7$ exhibited less toxicity and more potent anti-cancer effects than DDP. Thus, $C_{24}H_{20}N_2O_7$ may be a promising and potential antitumor drug with low toxicity and high efficiency for the clinical management of several types of cancer.

This is the first study to explore the anticancer activity of $C_{24}H_{20}N_2O_7$. In this study, we are simply trying to assess the anticancer effects of $C_{24}H_{20}N_2O_7$ on liver cancer and determine a direction for further study of the underlying anticancer mechanism. We intend to explore the specifics of the anticancer mechanism in future studies based on the findings presented in this manuscript.

Acknowledgement

The present study was supported by the National Natural Science Foundation of China (grant no. 81760538).

Conflict of interest

The authors declare no conflict of interest.

References

1. Sung H, Ferlay J, Siegel RL, Laversanne M, Soerjomataram I, Jemal A, Bray F, Global Cancer Statistics 2020: GLOBOCAN Estimates of Incidence and Mortality Worldwide for 36 Cancers in 185 Countries. *CA Cancer J Clin.*, 2021; 71(3): 209-249.
2. Feng RM, Zong YN, Cao SM, Xu RH, Current cancer situation in China: good or bad news from the 2018 Global Cancer Statistics?. *Cancer Commun.*, 2019; 39(1): 22.
3. Li B, Zhang W, Tan T, Liu W, Luo X, Zhang J, Yang Y, Li R, Ge Z, Chinese Herbal Formulas Miao-Yi-Ai-Tang Inhibits the Proliferation and Migration of Lung Cancer Cells through Targeting β-Catenin/ AXIN and Presents Synergistic Effect with Cisplatin Suppressing Lung Cancer. *Biomed Res Int.*, 2020; 2020: 2761850.
4. Newman DJ, Modern traditional Chinese medicine: Identifying, defining and usage of TCM components. *Adv Pharmacol.*, 2020; 87: 113-158.
5. Zhao J, Yang J, Xie Y, Improvement strategies for the oral bioavailability of poorly water-soluble flavonoids: An overview. Int J Pharm., 2019; 570: 118642.
6. Shao H, Li B, Li H, Gao L, Zhang C, Sheng H, Zhu L, Novel Strategies for Solubility and Bioavailability Enhancement of Bufadienolides. *Molecules*, 2021; 27(1): 51.
7. Qu Q, He Z, Jiang Y, Lu D, Long X, Ding Y, Xu B, He X, $C_{18}H_{17}NO_6$ Inhibits Invasion and Migration of Human MNNG Osteosarcoma Cells via the PI3K/ AKT Signaling Pathway. *Med Sci Monit.*, 2019; 25: 7527-7537.
8. He XY, Xiong LL, Xia QJ, Wang YY, Zhao XM, Du RL, Huang J, He XQ, Wang TH, $C_{18}H_{17}NO_6$ and Its Combination with Scutellarin Suppress the Proliferation and Induce the Apoptosis of Human Glioma Cells via Upregulation of Fas-Associated Factor 1 Expression. *Biomed Res Int.*, 2019; 2019: 6821219.
9. Sitohy M, Chobert JM, Haertlé T, Improvement of solubility and of emulsifying properties of milk proteins at acid pHs by esterification. *Nahrung*, 2001; 45(2): 87-93.
10. Lian WJ, He XQ, Zhao Q, Wang YT, Wu Y, You YT, Sythesis and antitumor activity of usnea nicotinyl amine. *Journal of Kunming Medical University*, 2020; 41: 1-5.
11. Kim D, Langmead B, Salzberg SL, HISAT: a fast spliced aligner with low memory requirements. *Nat Methods.*, 2015; 12(4): 357-360.
12. Pertea M, Kim D, Pertea GM, Leek JT, Salzberg SL, Transcript-level expression analysis of RNA-seq experiments with HISAT, StringTie and Ballgown. Nat Protoc., 2016; 11(9): 1650-1667.
13. Pertea M, Pertea GM, Antonescu CM, Chang TC, Mendell JT, Salzberg SL, StringTie enables improved reconstruction of a transcriptome from RNA-seq reads. *Nat Biotechnol.*, 2015; 33(3): 290-295.
14. Ashburner M, Ball CA, Blake JA, Botstein D, Butler H, Cherry JM, Davis AP, Dolinski K, Dwight SS, Eppig JT, Harris MA, Hill DP, Issel-Tarver L, Kasarskis A, Lewis S, Matese JC, Richardson JE, Ringwald M, Rubin GM, Sherlock G, Gene ontology: tool for the unification of biology. The Gene Ontology Consortium. *Nat Genet.*, 2000; 25(1): 25-29.
15. The Gene Ontology Consortium. The Gene Ontology Resource: 20 years and still Going strong. *Nucleic Acids Res.*, 2019; 47(D1): D330-D338.
16. Kanehisa M, Post-genome Informatics, Oxford University Press, 2000.
17. Lee J, Kim K, Son J, Lee H, Song JH, Lee T, Jeon H, Kim HS, Park SJ, Yoo HY, Park C, Improved Productivity of Naringin Oleate with Flavonoid and Fatty Acid by Efficient Enzymatic Esterification. *Antioxidants*, 2022; 11(2): 242.
18. Taghizadehghalehjoughi A, Hacimuftuoglu A, Cetin M, Ugur AB, Galateanu B, Mezhuev Y, Okkay U, Taspinar N, Taspinar M, Uyanik A, Gundogdu B, Mohammadzadeh M, Nalci KA, Stivaktakis P, Tsatsakis A, Jung TW, Jeong JH, Abd El-Aty AM, Effect of metformin/irinotecan-loaded poly-lactic-co-glycolic acid nanoparticles on glioblastoma: *in vitro* and *in vivo* studies. *Nanomedicine*, 2018; 13(13): 1595-1606.

19. Dobrzynska M, Napierala M, Florek E, Flavonoid Nanoparticles: A Promising Approach for Cancer Therapy. *Biomolecules*, 2020; 10(9): 1268.
20. Anton A, Moacă EA, Sarau CA, Dinu Ș, Semenescu AD, Macașoi IG, Dehelean CA, Antioxidant and *in vitro* cytotoxic activity of commercial lemongrass, sea buckthorn and basil essential oils, against colorectal cancer cell line HCT 116. *Farmacia*, 2022; 70(4): 683-689.
21. Chu Y, Kang Y, Yan C, Yang C, Zhang T, Huo H, Liu Y, LUBAC and OTULIN regulate autophagy initiation and maturation by mediating the linear ubiquitination and the stabilization of ATG13. *Autophagy*, 2021; 17(7): 1684-1699.
22. Huang C, Huang W, Ji P, Song F, Liu T, Li M, Guo H, Huang Y, Yu C, Wang C, Ni W, A Pyrazolate Osmium(VI) Nitride Exhibits Anticancer Activity through Modulating Protein Homeostasis in HepG2 Cells. *Int J Mol Sci.*, 2022; 23(21): 12779.
23. Nicco C, Batteux F, ROS Modulator Molecules with Therapeutic Potential in Cancers Treatments. *Molecules*, 2017; 23(1): 84.
24. Liu J, Yao L, Zhang M, Jiang J, Yang M, Wang Y, Downregulation of LncRNA-XIST inhibited development of non-small cell lung cancer by activating miR-335/SOD2/ROS signal pathway mediated pyroptotic cell death. *Aging*, 2019; 11(18): 7830-7846.
25. Chen X, Cubillos-Ruiz JR, Endoplasmic reticulum stress signals in the tumour and its microenvironment. *Nat Rev Cancer*, 2021; 21(2): 71-88.
26. Shi L, Fang J, Implication of heme oxygenase-1 in the sensitivity of nasopharyngeal carcinomas to radiotherapy. *J Exp Clin Cancer Res.*, 2008; 27(1): 13.
27. Prutianu I, Căruntu ID, Manole MB, GIușcă SE, Profire B, Timofte AD, Profire L, Gafton B, Developments in prostate cancer therapy: from the androgen receptor to antiandrogens and beyond. *Farmacia*, 2021; 69(3): 389-398
28. Jiang Y, Sun Y, Hu J, Yu N, Liu H, Fan J, Ning X, Li Y, Liu B, Sun Y, Zhang J, Qiu X, Fu S, Zhou C, Xu H, A germline mutation in Rab43 gene identified from a cancer family predisposes to a hereditary liver-colon cancer syndrome. *BMC Cancer.*, 2019; 19(1): 613.
29. Yu Q, Pu SY, Wu H, Chen XQ, Jiang JJ, Gu KS, He YH, Kong QP, TICRR Contributes to Tumorigenesis Through Accelerating DNA Replication in Cancers. *Front Oncol.*, 2019; 9: 516.
30. Lin XJ, Liu H, Li P, Wang HF, Yang AK, Di JM, Jiang QW, Yang Y, Huang JR, Yuan ML, Xing ZH, Wei MN, Li Y, Shi Z, Ye J, miR-936 Suppresses Cell Proliferation, Invasion, and Drug Resistance of Laryngeal Squamous Cell Carcinoma and Targets GPR78. *Front Oncol.*, 2020; 10: 60.